Clim Dyn (2013) 41:901–916
DOI 10.1007/s00382-012-1543-5

Quasi-stationarity of centennial Northern Hemisphere midlatitude winter storm tracks

Lan Xia · Hans von Storch · Frauke Feser

Received: 2 May 2012 / Accepted: 24 September 2012 / Published online: 5 October 2012

Abstract The winter storm activity on the Northern Hemisphere during the last one thousand years in a global climate simulation was analyzed by determining all midlatitude storms and their tracks, then consecutively clustering them for hundred years' segments. Storm track clusters with longest lifetime and largest deepening rates are found over the oceans. The numbers of extratropical winter storms exhibit notable yearly variability but hardly any variability on centennial time scales. The clusters of these storm tracks also show only small differences between the centuries. The numbers of members in neighboring oceanic clusters are negatively correlated. A linear relationship was found between the numbers of members per storm track clusters over the Pacific or Atlantic Ocean and seasonal mean atmospheric circulation patterns by a canonical correlation analysis.

1 Introduction

There is great interest in the issue of changing statistics of extratropical cyclones because of the impacts associated with the passage of such storms, in particular related to strong wind and heavy precipitation. Therefore many studies deal with perspectives of changing storm statistics in the course of emerging anthropogenic climate change (e.g. Schubert et al. 1998; Ulbrich and Christoph 1999; Pinto et al. 2007). However, for assessing the significance of expected future changes, knowledge about the natural variability of storminess is needed (IDAG 2005). But most analysis of recent and ongoing change of extratropical storm activity concentrated on recent decades re-analyses such as Sickmöller et al. (2000) and Weisse et al. (2005), or on the last century such as Alexandersson et al. (1998) and Matulla et al. (2008) who made use of proxies based on air pressure statistic. Only Fischer-Bruns et al. (2005) examined multi-centennial data—from coupled atmosphere–ocean global climate model (GCM) simulations subject to estimated external (volcanic, solar and anthropogenic) forcing. They showed that the storm frequency had no noteworthy long-term trends until recently. In particular no obvious link between temperature variations and extratropical storm activity emerged. We examine in this paper a similar GCM simulation, this time extending for almost 1,000 years, and we study the statistics through the lens of regional clustering and frequency of storm tracks. It has been shown previously that the temperature variations simulated by the model (von Storch et al. 2004) is relatively strong, albeit within the range of what is considered plausible for the past millennium (Moberg et al. 2005), so that we may expect the model to simulate also the century-to-century variability of other quantities, such as mid-latitude storminess.

This study is based on the availability of millennial simulations, which by now are routinely computed after their first appearance in the late 1990s (von Storch et al. 1997). This long simulation mostly operates with spatial resolutions which are suitable for extratropical storms, but not for tropical cyclones. Since it has been used and examined by various researchers on midlatitude storms (Fischer-Bruns et al. 2005), we limit ourselves to such midlatitude baroclinic storms.

Unfortunately, the spatial resolution of this simulation is relatively coarse, namely T30, and the output is stored only every 12 h. Jung et al. (2006) state that extratropical

L. Xia (✉) · H. von Storch · F. Feser
Institute of Coastal Research, Helmholtz-Zentrum Geesthacht, Geesthacht, Germany
e-mail: lan.xia@hzg.de

cyclone numbers within low horizontal resolution model data are 40 % smaller compared with reanalysis data. Uncertainties of cyclone frequency also rise due to the coarse temporal resolution (Zolina and Gulev 2002). However, previous analyses have employed just this configuration, such as Raible and Blender (2004) and Fischer-Bruns et al. (2005). When assessing storm activity in terms of variance of 500 hPa height, Stendel and Roeckner (1998) found that T30 generates reasonable patterns and the deviations are less than 10 % compared to ERA/ECMWF reanalysis data. A comparison of our results with other tracking studies is difficult as different tracking methods use different settings. Important is, however, that the spatial patterns and the relative frequencies of the different tracks are comparable. The intention of this study is to determine and discuss the variability of storm tracks from century to century. We argue that the underestimation of the total number and length of tracks acts in the same way throughout the simulation: our track numbers may be biased negatively, but uniformly, so that the variability should hardly be affected.

Various automatic tracking algorithms for describing cyclone activity in long-term datasets are available (Murray and Simmonds 1991; Hodges 1994, 1995; Serreze 1995; Blender et al. 1997; Muskulus and Jacob 2005; Wernli and Schwierz 2006; Rudeva and Gulev 2007; Zahn and von Storch 2008a). We adopt in our study Hodges (1994, 1995, 1999) well-documented and frequently applied method. The cluster analysis was developed for sorting objects into different categories, and can of course be applied to cyclones, e.g. Blender et al. (1997) and Sickmöller et al. (2000) for North Atlantic baroclinic storms, Elsner (2003), Nakamura et al. (2009) and Chu et al. (2010) for tropical storms.

How storm track activity relates to changes of circulation has been studied often: the effect of the North Atlantic Oscillation (NAO) (Hurrell 1995; Ulbrich and Christoph 1999; Gulev et al. 2001; Pinto et al. 2007; Raible et al. 2007) on storm statistics has been studied; also the effects of the Southern Oscillation (SO) (Sickmöller et al. 2000), the North Pacific Oscillation (PNA) (Christoph and Ulbrich 2000; Sickmöller et al. 2000; Gulev et al. 2001) as well as anomalies of midlatitude sea surface temperature (SST) anomalies (Brayshaw et al. 2008). In this paper, variability of Northern Hemisphere extratropical storms and its relation to changes in winter circulation is studied. This is done with the help of a Canonical Correlation Analysis of seasonal anomalies of mean sea level pressure fields (MSLP) and the time-variable number of members in the storm track clusters.

The long-term simulation dataset, obtained with the coupled atmosphere–ocean GCM ECHO-G exposed to time variable solar, volcanic and greenhouse-gas forcing of the last millennium, is described in Sect. 2. In Sect. 3.1 tracking results using the Lagrangian-type tracking algorithm of Hodges (1994, 1995 and 1999) are shown and compared with results derived from NCEP/NCAR reanalysis data in order to evaluate the model simulation. Time series of cyclone numbers for the 990 years (quasi-millennium) and for the 10 centuries are also shown. In Sect. 3.2 tracks are clustered into ten groups by the K-means clustering method; characteristics such as life span, frequency, or intensity are analyzed for each cluster. Century-to-century variability of cyclones for each cluster is also analyzed. Interactions of storm counts between different clusters are studied in Sect. 3.3. Variations of the numbers of members of the clusters in the marine sectors of the North Pacific and North Atlantic are related to mean winter circulation anomalies in Sect. 3.4. In Sect. 4 results are discussed and conclusions are drawn.

2 Data and methods

2.1 Data

The quasi-millennial (years 1000–1990) simulation which data is used in this study has been run with the global climate model ECHO-G (Min et al. 2005a, b) that combines the atmospheric model ECHAM4 (Roeckner et al. 1996) and ocean model HOPE-G (Wolff et al. 1997). For the atmospheric part the horizontal resolution is T30 (about 3.75°) and for the ocean T42 (about 2.8°). There are 19 (20) levels for the atmosphere (ocean). The output is stored every 12 h. The estimated historical forcing for driving the model such as solar variations, CO_2 and CH_4 concentrations as well as volcanic effects have been described previously by von Storch et al. (2004) and Zorita et al. (2005). ECHO-G simulations have been found skillfully in simulating the seasonal mean climatology and inter-annual variability of mean sea level pressure and surface temperature (Min et al. 2005a, b; Gouirand et al. 2007). The atmospheric circulation of the Northern Hemisphere in winter including the NAO pattern is simulated realistically by ECHO-G (Min et al. 2005b). The North Atlantic sea level pressure anomalies and response to the El Nino Southern Oscillation (ENSO) are similar to observed patterns and other climate reconstructions (Gouirand et al. 2007).

Examinations of shorter simulations done with ECHO-G have shown that the grid resolution of T30 is sufficient to study midlatitude baroclinic cyclones (Stendel and Roeckner 1998; Raible and Blender 2004; Fischer-Bruns et al. 2005). The storm tracks were found to agree well with ERA-15/ECMWF reanalysis data (Stendel and Roeckner 1998).

The key added value of this simulation is the homogeneous presentation of a possible development during the last millennium; obviously a validation of the simulation is hardly possible. However, with respect to the development of Northern Hemisphere temperature, comparisons with different proxy reconstructions are possible, ranging from tree ring data to borehole temperatures (González-Rouco et al. 2003, Tan et al. 2009). These indicate that this simulations is within the envelope of suggestions of past temperature development. Other simulations extending over 1,000 and more years also exhibit qualitatively similar developments. Some have argued that ECHO-G temperature variations would be too strong, however, which would not question our main conclusion namely that the mid-latitude winter storm activity is remarkably stationary on time scales of 100 years (see below).

2.2 Cyclone tracking

For cyclone identification and tracking, the automatic tracking algorithm developed by Hodges (1994, 1995 and 1999) is applied. This algorithm has widely been used to study climatology of extratropical cyclones (Hoskins and Hodges 2002, 2005), tropical storms and monsoon depressions (Hodges 1999), or specific cyclones such polar lows (Xia et al. 2012). In this study, only winter cyclones (DJF) at mid-latitudes (≥30°N) on the Northern Hemisphere (NH) are considered.

The tracking is done with mean sea level pressure (MSLP) fields of ECHO-G simulation. Before tracking, wavenumbers less than or equal to 5 are subtracted for removing large-scale features (Hoskins and Hodges 2002). Then the tracking algorithm determines all minima below -1 hPa in the filtered MSLP fields. Minima are connected to form tracks if their distance is less than 12° (about 1,333 km) within 12 h. Minimum lifetimes of tracks are set to 2 days.

For the temporal resolution, no ad-hoc process is used to interpolate the 12-hourly MSLP fields into shorter time steps (as e.g. Murray and Simmonds 1991; Zolina and Gulev 2002 have done). For getting smooth tracks, B-spline interpolation (Dierckx 1981, 1984) is used to overcome the coarseness of T30 (Hodges 1994, 1995). A smoothing procedure is also applied as suggested by Hodges (Hodges 1994, 1995). This procedure minimizes along-track variations in direction and speed. The smoothing is done adaptively, and is more invasive when the system moves slowly and less invasive when the systems moves fast (Hodges 1999).

2.3 Clustering analysis

Before clustering, processing is required so that the tracks are described by only a few characteristic parameters. Different approaches have been used to that end. For instance, Blender et al. (1997) used the relative displacement of a cyclone from its initial positions within 3 days. Elsner et al. (2000), dealing with hurricanes, used latitude and longitude coordinates at the positions of maximum and final intensities. Nakamura et al. (2009) used the location of maximum wind intensity of the storm track and variance ellipse which measures the shape of the cyclone track. Chu et al. (2010) fitted a second-order polynomial function to the tracks.

Here we adopt Chu et al.'s (2010) procedure and fit to each track a second-order polynomial function with six free parameters. The zero-order coefficients give the information about the genesis locations of a track; the first-order coefficients describe the direction of track; and the second-order terms represent the curvature of the track. Every track can be described by these six parameters and the clustering is done in this 6-dimensional space.

Then we cluster all tracks into ten groups by applying the K-means method to each century. The K-means method is applied widely for the cluster analysis (Blender et al. 1997; Elsner 2003; Nakamura et al. 2009). For k clusters, the K-means method minimizes the squared Euclidean distance S of cyclone tracks to their respective cluster centers.

$$S = \sum_{i=1}^{N} \sum_{j=1}^{L} (\beta_{i,j} - \mu_{k(i),j})^2,$$

where the N is the cyclone count, $\beta_{i,j}$ denotes the six second order polynomial parameters for each track i (L = 6). For the k-th cluster, the six-dimensional vector $\mu_{k,j}$ are the centroids of this cluster, which is made up of the means of the six parameters $\beta_{i,j}$ of all tracks i which belongs to the k-th cluster.

The K-means algorithm determines the clusters by iteratively swapping points between clusters to minimize S. The K-means algorithm could depend on the initial cluster centroid positions known as seeds. In order to minimize this dependency, the clustering was repeated 20 times, choosing a new set of track parameters as initial centroid positions each time (Blender et al. 1997). Sensitivity experiments have also been done within different cluster numbers k. The cluster number $k = 10$ was chosen in order to cover all cyclone genesis areas.

3 Results

3.1 Storm tracks

For validation purposes tracks obtained from the ECHO-G simulations are compared to those derived from NCEP/

NCAR reanalysis data (Kalnay et al. 1996). For doing so, NCEP/NCAR reanalysis data was interpolated into T30 and 12 hourly outputs, which are the same temporal and spatial resolution as ECHO-G, and tracked with the same settings. The numbers of tracks from the ECHO-G are at a similar level as those derived from this coarsened NCEP/NCAR reanalysis data. Densities for genesis regions representing the origins of storm tracks were compared (Fig. 1). Both sources describe the known genesis maxima for Pacific storms located over Mongolia, northeast of China, around southeastern China, east of Japan and in the central Pacific. This result is consistent with the studies by Adachi and Kimura (2007) and Inatsu (2009). Genesis maxima of Atlantic storms are located over continental America in the lee of the northern Rocky Mountains, along the coast of the United States and around Iceland, in accordance to Hoskins and Hodges (2002). Further genesis regions are found over the Norwegian Sea, over the western Mediterranean and over the Caspian Sea. In general, the distributions of genesis density in the ECHO-G simulation data agree with those derived from the NCEP/NCAR reanalysis data quite well.

Cyclone density is defined as winter (DJF) cyclone occurrences per area of 218,000 km^2 (Fig. 2). Figure 2a shows the mean winter storm density for the period from 1951 to 1990 with coarsened NCEP/NCAR reanalysis data and Fig. 2b is the difference between the ECHO-G simulation data and coarsened NCEP/NCAR reanalysis data. The maxima can be found in the western Pacific, in the Gulf of Alaska over North Pacific, along the coast of North America, in the southeast of Greenland and Barents Sea. For ECHO-G simulation data, the cyclone density over the Gulf of Alaska, in the south of Greenland, and Western Europe is larger, while it is smaller in southeast China, over the east of Japan and in the western Mediterranean Sea (Fig. 2b). But the differences are not large and the cyclone density pattern agrees with other results (Gulev et al. 2001; Hoskins and Hodges 2002). So we conclude that the midlatitude cyclone statistics generated from the ECHO-G simulation data are realistic.

The 990-year time series of winter cyclone numbers for the NH are shown in Fig. 3. Average cyclone numbers in each century are shown in Fig. 4. The smallest average cyclone number of 179/year is in the twentieth century (1901–1990). Also in the thirteenth (1201–1300) and fourteenth (1301–1400) century relatively few storms are counted, with 180 per year. Highest numbers (182 counts per year) emerge in the fifteenth (1401–1500) century. But generally the average cyclone frequency for different centuries is quite similar with little variability (Fig. 4), while the year-to-year variations for storm numbers are strong (Fig. 3). Long-term trends can not be detected during the quasi-millennial winters of years 1001–1990.

This result is very similar to that of Fischer-Bruns et al. (2005) who used the maximum wind speed to define storm days based on a shorter ECHO-G simulation. They compared the storm day frequency between pre-industrial times (1551–1850) and industrial times (1851–1990) and found no noticeable differences. They stated that during historical times storms statistics for both hemisphere are remarkably stable with little variability and storminess mostly decoupled from temperature variations. Only in the climate change scenarios, which describe possible developments in

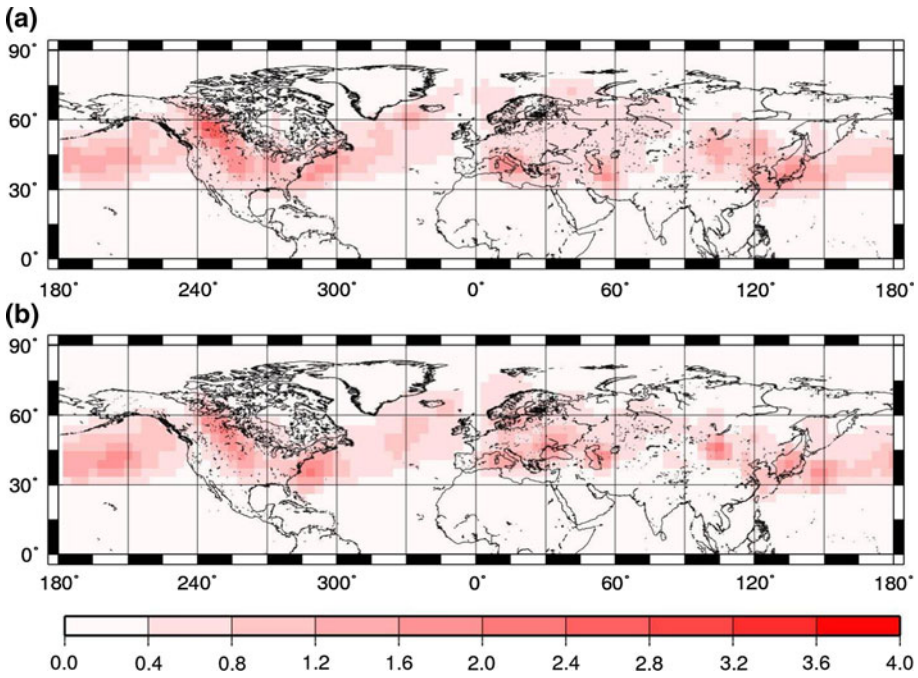

Fig. 1 40-years (1951–1990) average density distribution of cyclone genesis in winter for the Northern Hemisphere: **a** coarsened NCEP/NCAR reanalysis data; **b** ECHO-G simulation data

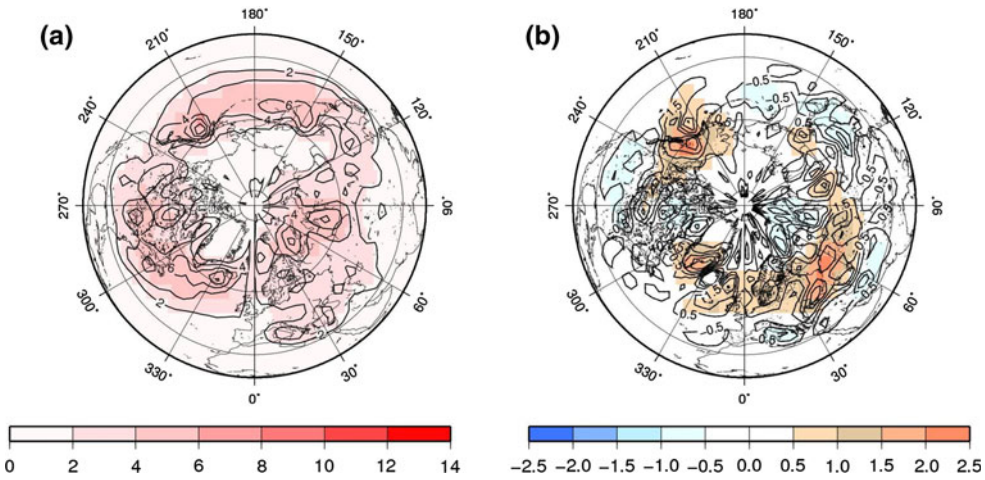

Fig. 2 40-years (1951–1990) mean cyclone density (unit: cyclones/winter per 218000 km^2) for the Northern Hemisphere: **a** coarsened NCEP/NCAR reanalysis data; **b** difference between ECHO-G simulation data and coarsened NCEP/NCAR reanalysis data

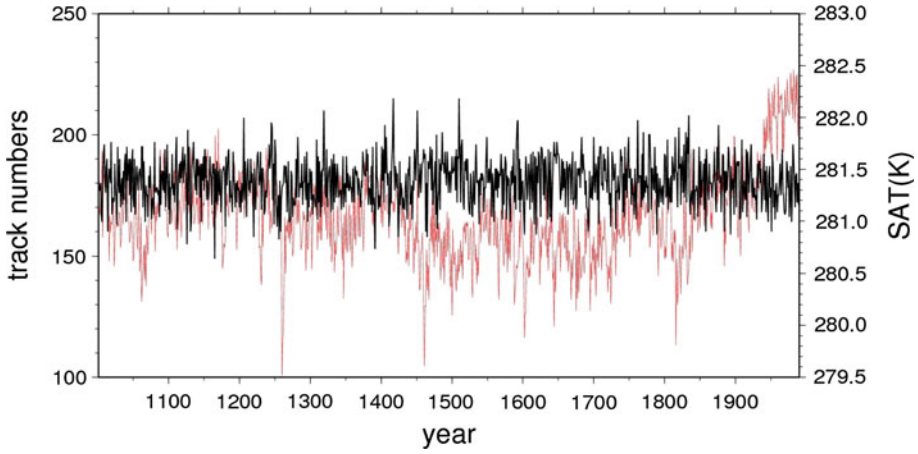

Fig. 3 Time series of the numbers of winter (DJF) extratropical cyclones (*black line*) and winter surface air temperature (SAT: K) (*red line*) in the Northern Hemisphere (NH) (years 1001–1990)

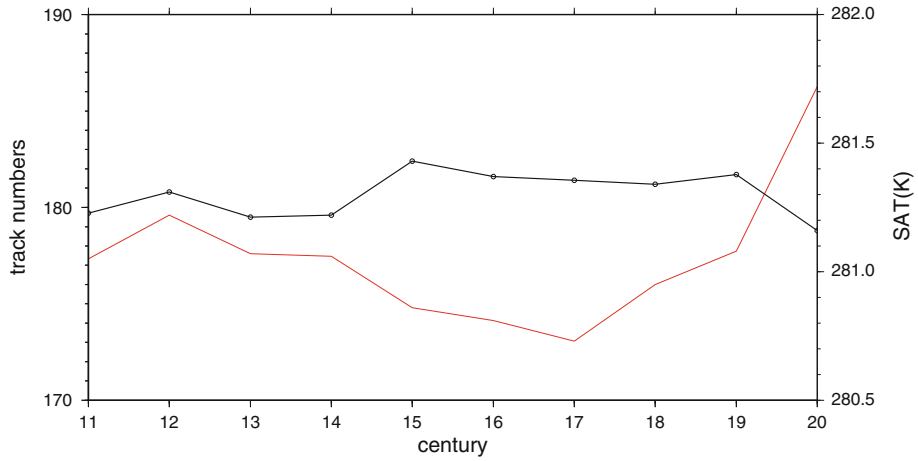

Fig. 4 Average annual numbers of winter (DJF) extratropical cyclones (*black line*) and average winter SAT (K) (*red line*) in the NH for different centuries (11th–20th century)

the twenty first century, with a strong increase of greenhouse gas concentrations, the distributions of high storm frequency exhibited a poleward shift. But there is no increase in the number of storms when the sum over the entire Northern Hemisphere is formed. Also here, we find the large variations in temperature not reflected in parallel variations of cyclone counts (Figs. 3 and 4).

However, compared to higher resolution, the track numbers derived from coarse temporal and spatial grids are underestimated (Blender and Schubert 2000; Jung et al. 2006; Zolina and Gulev 2002). According to the study of Jung et al. (2006), cyclones in the northern Pacific, the Arctic, Baffin Bay, the Labrador Sea and the Mediterranean Sea are specifically sensitive to the spatial resolution.

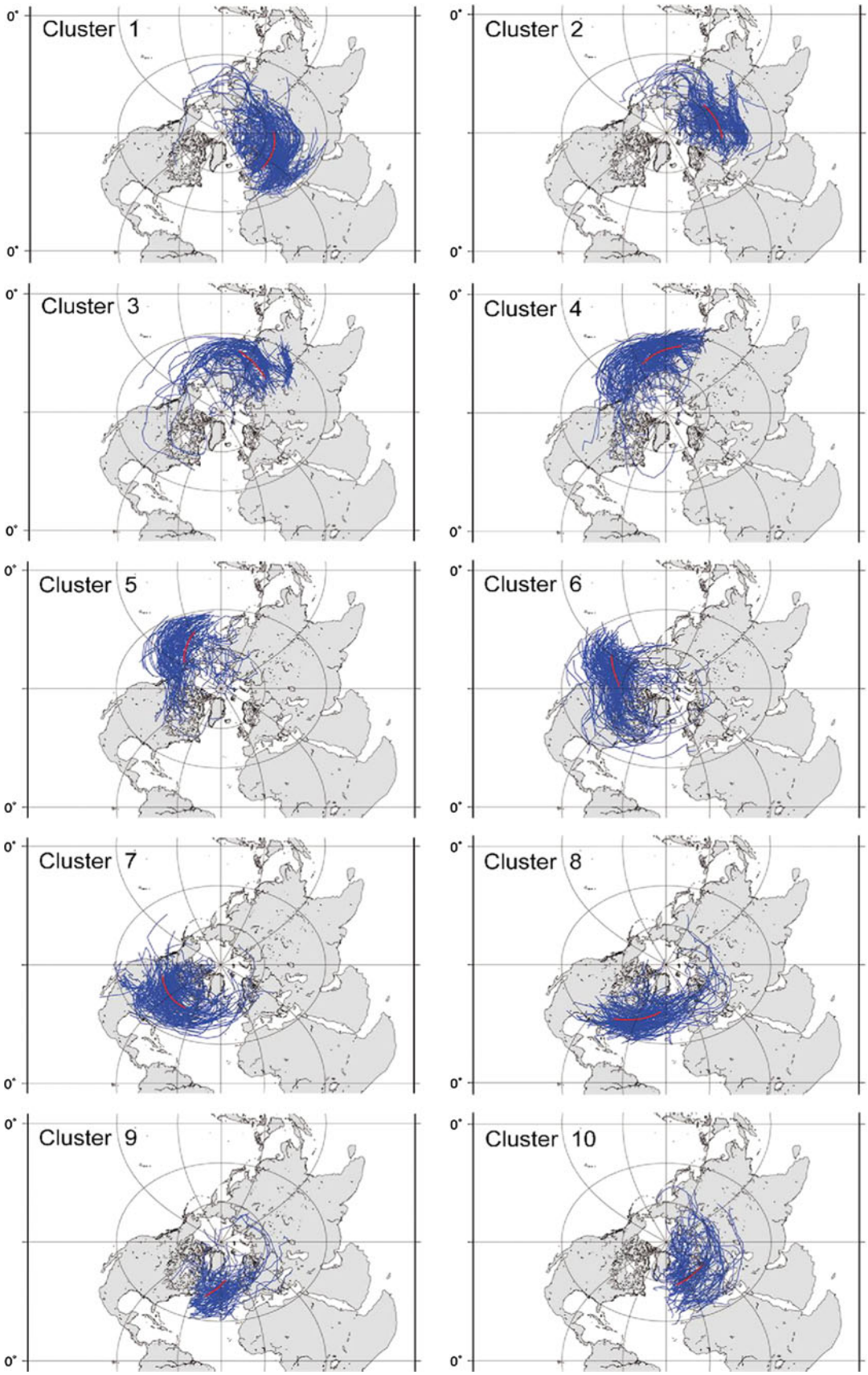
Cluster 1
Cluster 2
Cluster 3
Cluster 4
Cluster 5
Cluster 6
Cluster 7
Cluster 8
Cluster 9
Cluster 10

◀ **Fig. 5** Winter (DJF) extratropical cyclone tracks of the 20th century (years 1901–1990) in the NH clustered into ten clusters by applying the K-means method: member tracks (*blue*) and centroid tracks (*red*) of the ten clusters

Our results differ from what has been reported by Gulev et al. (2001)—the cyclone density of ECHO-G is up to 12 cyclones per winter per 218,000 km^2 (Fig. 2) which is less than the number given by Gulev et al. (2001) (up to 20 cyclones per winter per 218,000 km^2). This difference may partly be due to the different resolution or other deficits of the model ECHO-G, but it may also reflect different tracking settings of these two studies in determining storm tracks. More important is that the overall patterns and the relative frequencies are comparable.

3.2 Clustering results

All tracks were clustered into ten groups by applying the K-means method in each century (Fig. 5). The centroid track is the mean track of each cluster. We can see that the 10 clusters form a kind of midlatitude ring around the Northern Hemisphere (Fig. 5), with a poleward bend at their ends. It is similar to the schematic of principal tracks (Fig. 15 of Hoskins and Hodges, 2002) and consistent with the genesis areas (Fig. 1). Across the Pacific, tracks are separated into three clusters: cluster 4 from the southeast of China to the Japan Sea, cluster 5 from the east of Japan to the center of the Pacific, and cluster 6 in the eastern Pacific. In the Atlantic, there are also 3 clusters: cluster 8 from the eastern North American coast, cluster 9 from the southern Greenland, and cluster 10 extending from southeastern Iceland to the Norwegian Sea. Cluster 7 corresponds to the tracks generated from continental American in the lee of the northern Rocky Mountains. The classifications in the Pacific and Atlantic are quite similar to those of Gulev et al. (2001) except that only two clusters appear for the Pacific.

Table 1 lists the numbers of tracks per cluster for the whole time period 1001–1990. Cluster 1 which emanates from the North Sea, Baltic Sea and the western Mediterranean has the most members. In the Pacific, the eastern cluster 6 has the highest numbers of tracks, while the central cluster 5 has the fewest. Over the Atlantic, the western cluster 8 has the most tracks, whereas the fewest number is found in the central cluster 9. The sum of cyclone counts for the three Pacific clusters (4, 5, 6) is larger than that for the three Atlantic clusters (8, 9, 10).

Many studies found tracks or track density shift northward in the future greenhouse gas forcing (Schubert et al. 1998; Ulbrich and Christoph 1999; Fischer-Bruns et al. 2005; Pinto et al. 2007). Observation from satellite also supports that the storm cloudiness has a poleward shift (Bender et al. 2012). Figure 6 displays the centroid (mean) tracks of the ten clusters for the earliest 11th century (years 1001–1100) and the latest 20th century (years 1901–1990). They differ very little. Obviously, the geometric positions of the tracks were quite similar in the first and last century of the last millennium. The results of Fischer-Bruns et al. (2005) indicate that it is not the hemispheric temperature, which is related to the change in tracks, but other factors, such as the zone of maximum baroclinicity.

Figure 7 shows the average cyclone numbers for the 10 clusters in different centuries. There are no large variations between different centuries; the large differences in cyclone counts between the clusters vary very little from century to century. Some may expect systematic changes, at least over the North Atlantic for centuries, when regional significant temperature anomalies prevail, such as the Medieval Warm Period (AD 950–1250) and the Little Ice Age (AD 1500–1700) (Keigwin 1996, KIHZ-Consortium 2004)—however, the differences are rather small (Fig. 7: cluster 8, 9 and 10). Fischer-Bruns et al. (2005) stated that the variations of storm activity are not linearly related to temperature variability during historical times in the ECHO-G simulation.

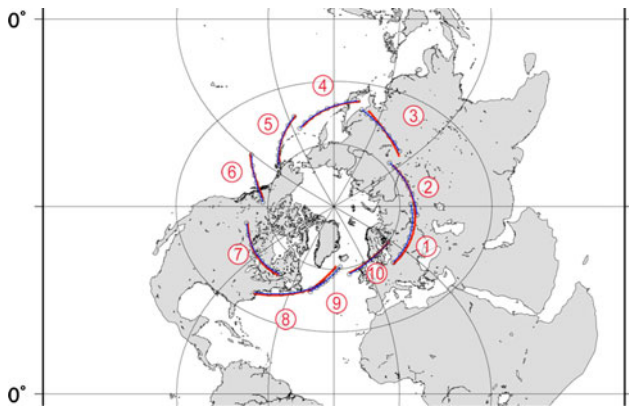

Fig. 6 Mean tracks of ten clusters (*red numbers*) for the NH in the 11th and 20th century: *red* ones are the mean tracks of the ten clusters in the11th century (years 1001–1100), *blue* ones with *circles* are the mean tracks of the ten clusters in the 20th century (years 1901–1990)

Table 1 Cyclone numbers of the ten clusters shown in Fig. 5 for the quasi- millennial time period (years 1001–1990)

Cluster	1	2	3	4	5	6	7	8	9	10
Numbers	23,955	16,625	15,519	20,219	16,720	21,510	21,435	15,899	13,079	13,918

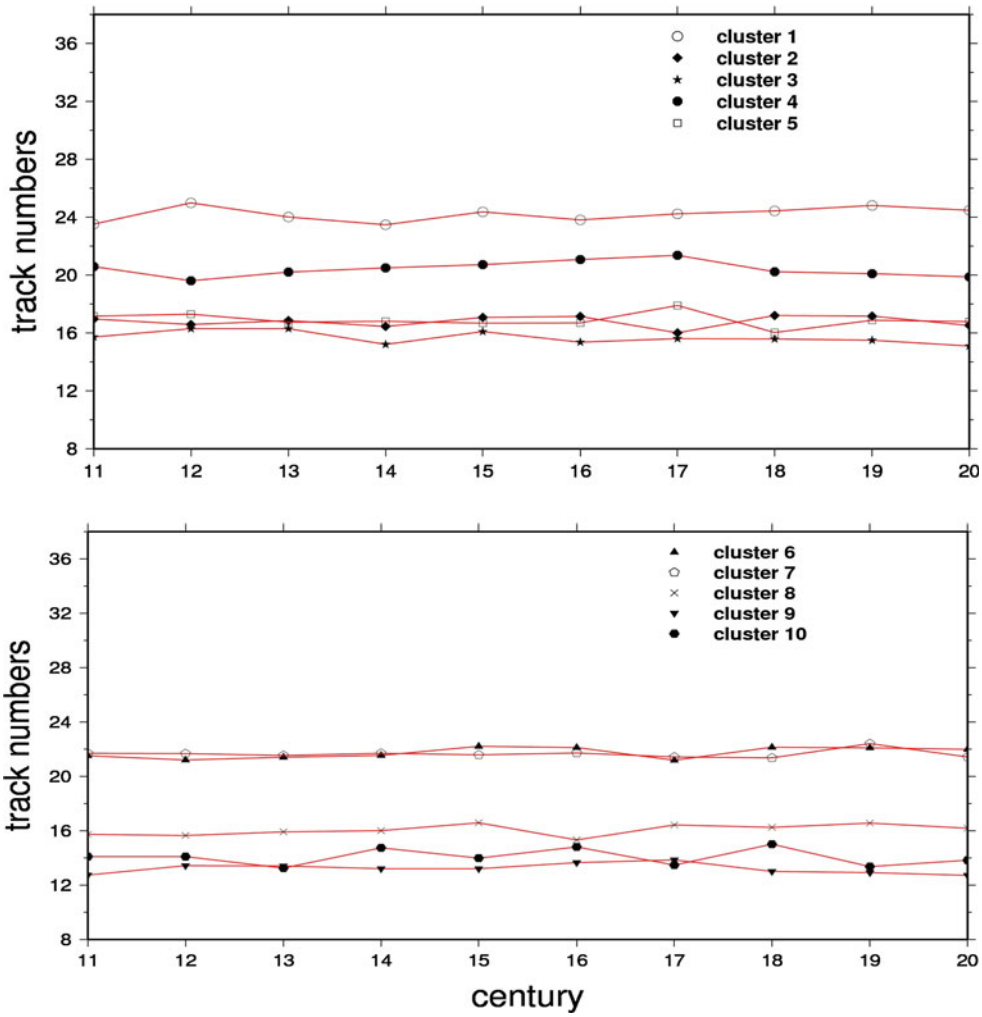

Fig. 7 Average annual numbers of winter (DJF) extratropical cyclones in the NH for the ten clusters in different centuries (11th–20th century)

Table 2 shows the distribution of lifetimes for all clusters. Overall, the highest percentage is found for the lifetimes of 2–4 days. For clusters 2, 3 and 6 over 60 % of tracks last 2–4 days. Cluster 8, primarily located over the eastern North American coast, contains most long-lived (more than 10 days) cyclones with about 7 % of all its cyclones (Table 2 and Fig. 8b). Over the Atlantic, the eastern cluster 10 which extends from southeastern Iceland to the Norwegian Sea, shows an average lifetime of about 5 days; also the number of long-lived cyclones (5.0 %) is a little larger than cluster 9. For the Pacific, cluster 4 has the highest percentage (5.6 %) of cyclones lasting more than 10 days with a mean lifetime of about 6 days (Fig. 8a). In general, cyclones travelling from land to the sea tend to

Table 2 Lifespan (days) distribution rates of the ten clusters shown in Fig. 5 for the quasi- millennial time period (years 1001–1990) (Unit: %)

Lifetime(days)	2–4	4–6	6–8	8–10	>10
Cluster 1	43.25	30.20	16.70	6.19	3.65
Cluster 2	60.82	25.86	7.99	3.04	2.29
Cluster 3	63.12	15.11	10.02	6.60	5.15
Cluster 4	36.02	28.98	19.96	9.40	5.64
Cluster 5	50.19	29.93	12.40	4.45	3.03
Cluster 6	60.38	24.42	8.51	3.84	2.86
Cluster 7	56.66	18.03	13.28	6.80	5.23
Cluster 8	39.10	29.74	16.48	7.72	6.96
Cluster 9	55.68	23.62	10.54	5.25	4.92
Cluster 10	47.96	24.68	14.59	7.77	5.01

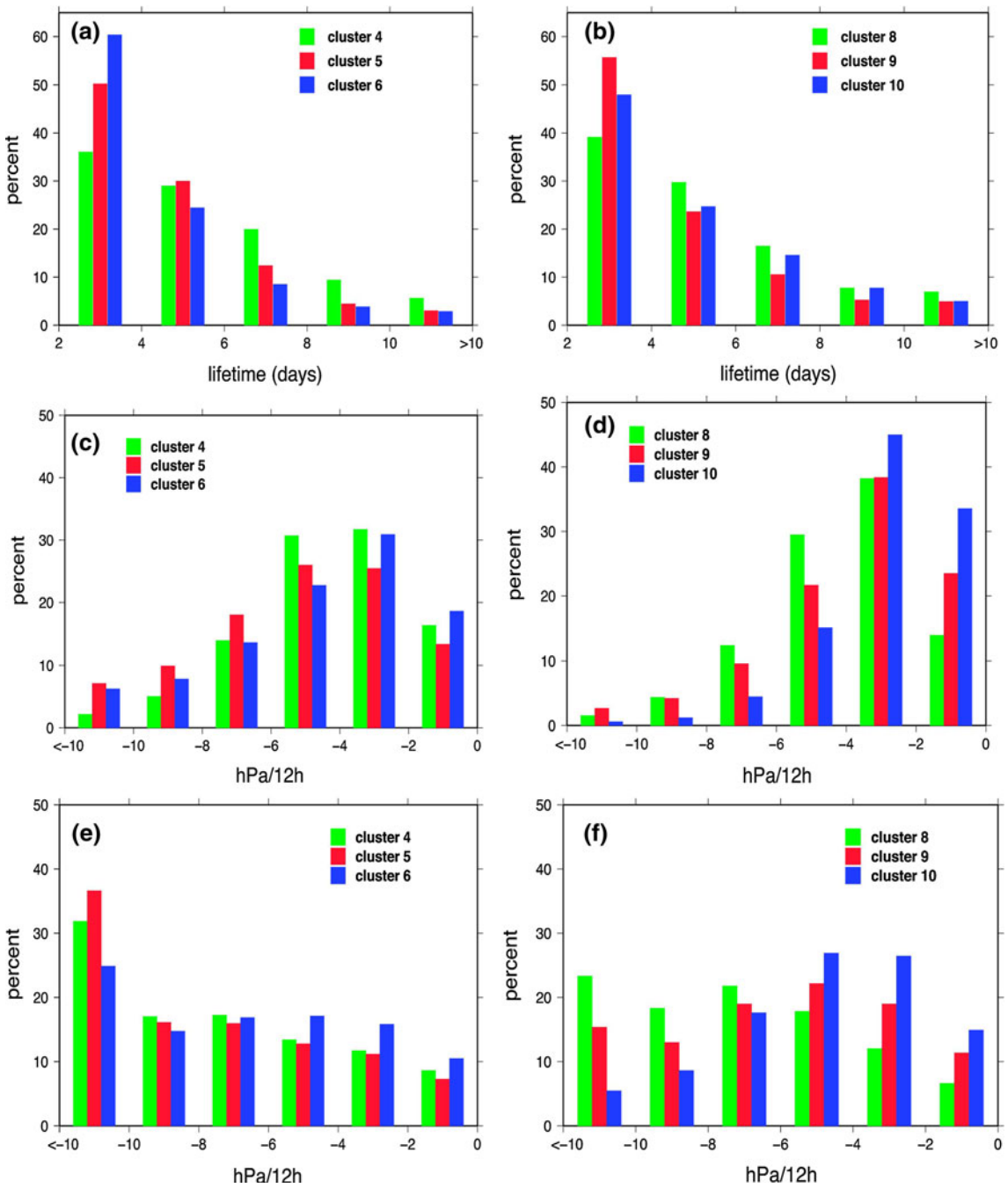

Fig. 8 Distributions (%) of cyclone lifetime (days) (**a** and **b**), mean deepening rates (hPa/12 h) (**c** and **d**), and maximum deepening rates (hPa/12 h) (**e** and **f**) for winter cyclones over the Pacific (**a**, **c** and **e**) and the Atlantic (**b**, **d** and **f**) for the whole time period (years 1001–1990)

exist for a longer time, such as those in clusters 3 and 7. The warm Kuroshio current in the Pacific and the Gulf stream in the Atlantic play important roles in generating baroclinic situations favoring the lasting of cyclones. Latent heat release and moisture over the ocean also contribute to the development of cyclones and make them survive longer.

Deepening rates for each track were determined, and frequency distributions for these rates for all tracks in a cluster derived. The "averaged" deepening rate is calculated for the period, from genesis location to the maximum pressure value; the "maximum" "deepening rate" is the largest pressure fall along a track. Table 3 shows the mean deepening rates per 12 h for the ten clusters for the whole time period 1001–1990. In the Atlantic, the average deepening rates are mainly between 2 and 4 hPa/12 h for clusters 8, 9, and 10 with 38.2, 38.4 and 45.0 %, respectively (Fig. 8d and Table 3). Cluster 8 for the eastern North

Table 3 Mean deepening rate (hPa/12 h) distributions of the ten clusters shown in Fig. 5 for the quasi- millennial time period (years 1001–1990) (Unit: %)

Mean deepening rates (hPa/12 h)	<−10	−10 to −8	−8 to −6	−6 to −4	−4 to −2	−2 to 0
Cluster 1	0.08	0.34	1.95	11.44	45.79	40.40
Cluster 2	0.07	0.27	1.52	9.01	38.62	50.51
Cluster 3	0.10	0.57	2.86	14.54	36.98	44.95
Cluster 4	2.15	5.05	13.99	30.70	31.69	16.42
Cluster 5	7.12	9.90	18.13	26.01	25.44	13.40
Cluster 6	6.23	7.83	13.65	22.73	30.92	18.63
Cluster 7	0.23	0.69	3.41	14.84	42.22	38.61
Cluster 8	1.55	4.37	12.40	29.49	38.19	14.00
Cluster 9	2.65	4.19	9.60	21.67	38.37	23.51
Cluster 10	0.59	1.22	4.45	15.17	45.00	33.56

American coast also shows an elevated average deepening rate of 4–6 hPa/12 h. In the Pacific, there are more cyclones with an average deepening rate of 4–6 hPa/12 h compared with Atlantic cyclones: especially cluster 4 in the western Pacific (30.7 %, Fig. 8c). In other clusters average deepening rates are mostly about 0–2 hPa/12 h, except for clusters 1 and 7 which have their largest deepening rate percentage between 2 to 4 hPa per 12 h (Table 3).

Table 4 lists the distributions of maximum deepening rates per 12 h. Figure 8e and f show maximum deepening rates for the Pacific and the Atlantic. In the Pacific, more than about 25 % of all cyclones go with a rapid maximum deepening rate of more than 10 hPa/12 h. Cluster 5 over the central Pacific has the highest maximum deepening rate (36.6 %) of more than 10 hPa per 12 h (Fig. 8e). Over the Atlantic, the maximum deepening rates of more than 10 hPa per 12 h occur less often than over the Pacific. Only cluster 8 over the eastern North American coast shows a maximum deepening rate over 10 hPa per 12 h for 23.4 % of all its cyclones (Fig. 8f). Cluster 9 (22.2 %) over southern Greenland, and cluster 10 (26.9 %), extending from southeastern Iceland to the Norwegian Sea, show mainly maximum deepening rates of 4–6 hPa/12 h. From the studies of Gulev et al. (2001) of NCEP/NCAR re-analysis and from Uccellini (1990) it is known that the largest deepening takes place over the oceans. Thus, the statistics of the ECHO-G cyclone clusters are found to be consistent with the previous analysis of "observed" cyclone activity.

Figure 9 shows changes of the maximum deepening rates for the Atlantic and Pacific clusters during different centuries. In the 20th century maximum deepening rates larger than 10 hPa per 12 h become less frequent for cluster 8 but more frequent for cluster 10 in the Atlantic (Fig. 9 right). Between the 17th and 18th century the maximum deepening rates for cluster 8 of 6–8 hPa per 12 h become more frequent, but those larger than 8 hPa per 12 h less frequent. There are tendencies of decreases in the frequency of deep cyclones in the 16th–17th and 19th century for cluster 9 and in the 16th and 19th century for cluster 10. In the Pacific, in the 20th century frequencies of rapidly deepening cyclones (over 10 hPa/12 h) slightly

Table 4 Maximum deepening rate (hPa/12 h) distributions of the ten clusters shown in Fig. 5 for the quasi- millennial time period (years 1001–1990) (Unit: %)

Maximum deepening rates (hPa/12 h)	<−10	−10 to −8	−8 to −6	−6 to −4	−4 to −2	−2 to 0
Cluster 1	2.27	5.58	15.03	28.81	32.05	16.26
Cluster 2	2.08	3.24	9.57	22.48	36.44	26.19
Cluster 3	9.31	7.15	10.76	16.89	28.23	27.66
Cluster 4	31.89	17.06	17.27	13.42	11.72	8.64
Cluster 5	36.64	16.12	15.96	12.78	11.18	7.31
Cluster 6	24.89	14.76	16.89	17.14	15.84	10.48
Cluster 7	9.45	8.78	14.33	19.74	24.68	23.03
Cluster 8	23.35	18.33	21.81	17.83	12.03	6.64
Cluster 9	15.38	13.01	19.01	22.18	19.02	11.39
Cluster 10	5.47	8.63	17.62	26.91	26.44	14.93

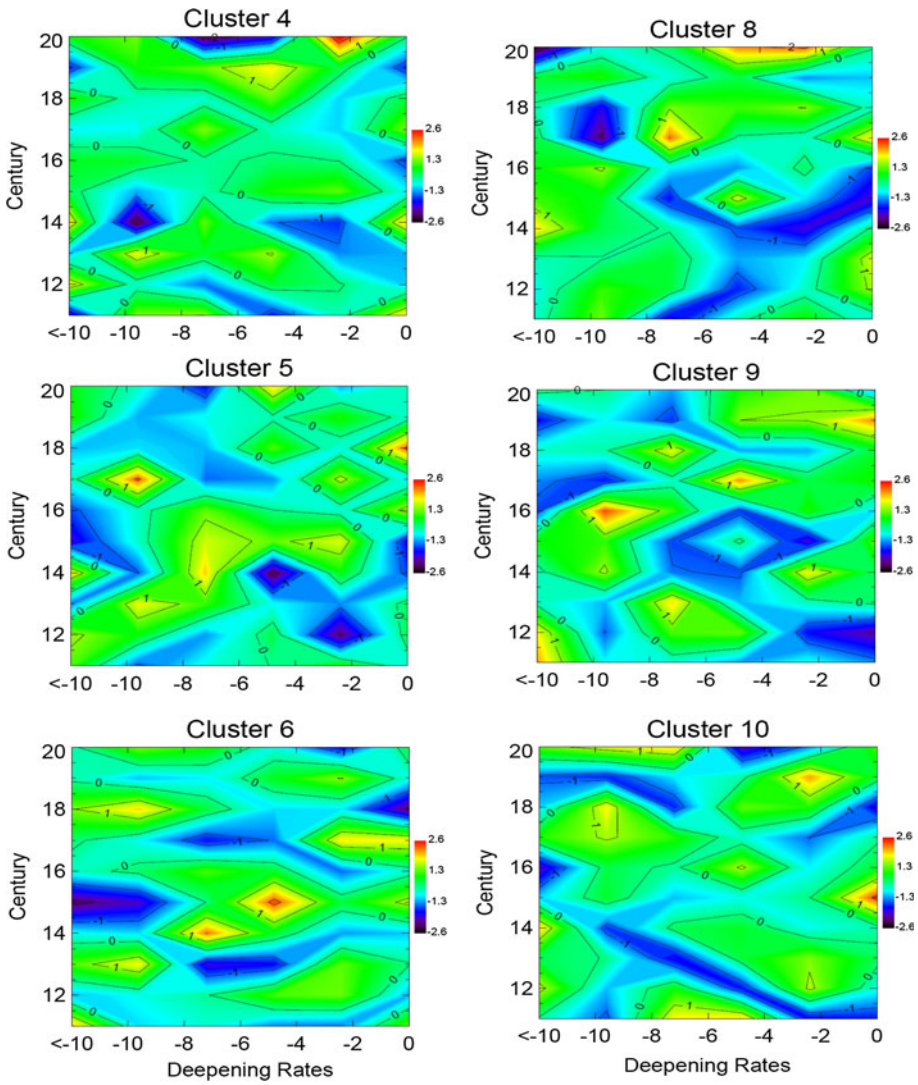

Fig. 9 Normalized anomalies of the maximum deepening rate distributions for cluster members over the Pacific (cluster 4, 5 and 6) and the Atlantic (cluster 8, 9 and 10) across different centuries (11th–20th century)

Table 5 Correlations of time series of winter cyclone numbers between the ten clusters shown in Fig. 5 (years 1001–1990): blue ones are correlation coefficients with a reliability of 95 % determined by a *t* test

clusters	2	3	4	5	6	7	8	9	10
1	-0.17	0.02	0.01	0	0.03	-0.02	-0.03	-0.01	-0.21
2		-0.04	0	0	0.01	-0.02	-0.03	0.06	-0.02
3			-0.11	-0.11	0.02	-0.08	0.02	0.03	-0.02
4				-0.22	-0.10	0.02	-0.03	0.01	0
5					-0.32	-0.09	0.09	-0.02	-0.04
6						-0.06	-0.12	0.13	0.11
7							-0.22	0.01	-0.01
8								-0.23	-0.10
9									0.01

increase for cluster 4 and 5 (Fig. 9 left), and relatively slowly deepening cyclones (2–4 hPa/12 h) appear more often in cluster 4 but less so in cluster 6. There are decreases in the frequency of deep cyclones in the 11th and 19th century for cluster 4, during the15th to 16th century for cluster 5, and in the 12th century and during the 14th to 16th century for cluster 6.

3.3 Interactions between clusters

Linkages between cyclonic activities in the Pacific and the Atlantic have been studied before (May and Bengtsson 1998, Sickmöller et al. 2000). Sickmöller et al. (2000) showed that the numbers of the north-eastward direction cyclones in the Pacific are related to the frequency of the

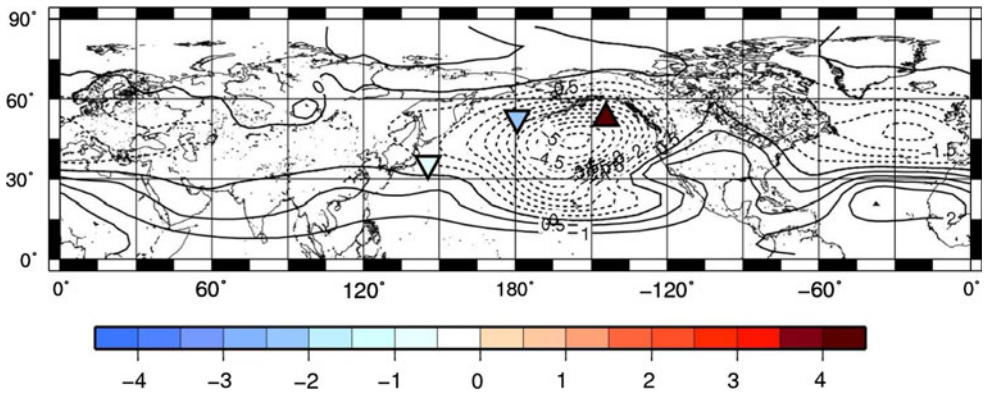

Fig. 10 Corresponding correlation patterns between time series of winter (DJF) cyclone numbers in the Pacific (clusters 4, 5 and 6) (*triangles*: for positive values, *inverted triangle* for negative values) and mean sea level pressure fields in hPa (*isolines*: *dashed* for negative and *solid* for positive). The first CCA pair shares a correlation coefficient of 0.59 and represents 48 % of the variance of winter cyclone numbers from year 1001 to 1990. Cyclone frequency anomalies are −0.6 for cluster 4, −2.2 for cluster 5, but 4.6 for cluster 6

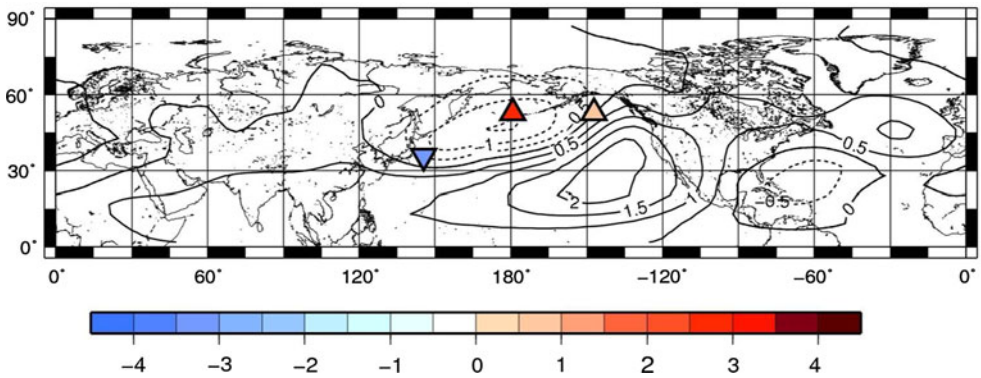

Fig. 11 Same as Fig. 10 for the second CCA pair: it shares a correlation coefficient of 0.39 and represents 35 % of the variance of winter cyclone numbers from year 1001 to 1990. Cyclone frequency anomalies are −3.2 for cluster 4, but 2.9 for cluster 5, and 0.6 for cluster 6

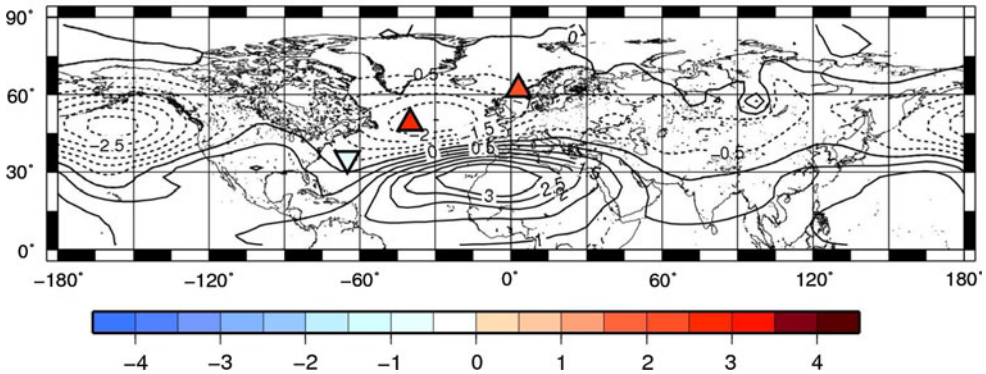

Fig. 12 Corresponding correlation patterns between time series of winter (DJF) cyclone numbers in the Atlantic (clusters 8, 9 and 10) (*triangles*: for positive values, *inverted triangle* for negative values) and mean sea level pressure fields in hPa (*isolines*: *dashed* for negative and *solid* for positive). The first CCA pair shares a correlation coefficient of 0.51 and represents 39 % of the variance of winter cyclone numbers from year 1001 to 1990. Cyclone frequency anomalies are −0.9 for cluster 8, but 3.0 for cluster 9, and 2.0 for cluster 10

north-eastward and zonal directional cyclones in the Atlantic. It was also suggested that upper-level Pacific depressions could cross North America and influence the genesis of cyclones over the western Atlantic.

We analyzed the correlations of the numbers between the ten clusters (Table 5), as derived from all 990 winters of the simulation. The main feature is a significant, albeit not large negative correlation between neighboring

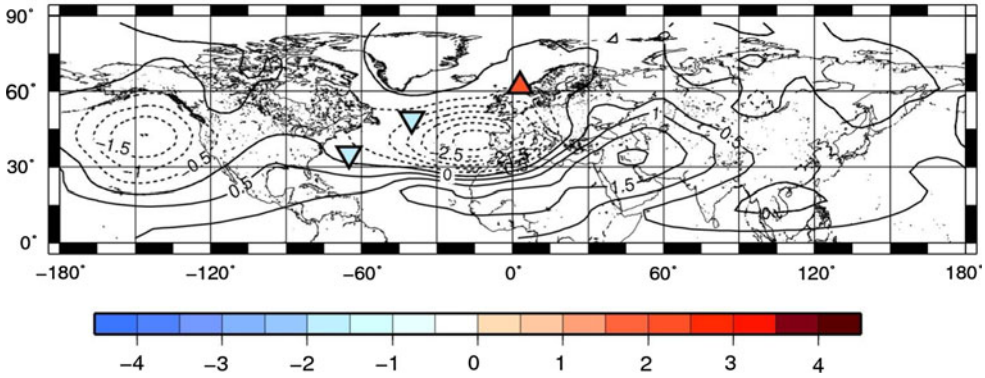

Fig. 13 Same as Fig. 12 for the second CCA pair: it shares a correlation coefficient of 0.27 and represents 31 % of the variance of winter cyclone numbers from year 1001 to 1990. Cyclone frequency anomalies are −1.7 for cluster 8 and −1.7 for cluster 9, but 2.3 for cluster 10

clusters, e.g. between the Atlantic clusters 8 and 9 (−0.23), the Pacific clusters 4/5 (−0.22) and 5/6 (−0.32), the continental clusters 7/8 (−0.22) and 1/10 (−0.21). Also minor correlations are found between non-neighboring clusters across the North American continent such as clusters 6/8 (−0.12), 6/9 (0.13), and 6/10 (0.11). Thus the linkage between neighboring clusters is not strong but a robust feature, while the remote linkages are very weak.

3.4 Links to large-scale pressure patterns

We investigate how seasonal (DJF) mean MSLP patterns are related to the yearly numbers of cyclones in the Pacific and the Atlantic. Canonical Correlation Analysis (CCA) (von Storch and Zwiers 1999) is used to determine systematic mutual dependencies in the yearly MSLP fields and yearly cyclone counts for the three clusters in the Pacific and the Atlantic separately. Prior to the CCA, a data compression was done truncating the high-dimensional MSLP fields to the first thirteen Empirical Orthogonal Functions (EOFs) (von Storch and Zwiers 1999). The fields, both EOF-truncated MSLP as well as cluster counts, are based on deviations from the long-term (990 winters) mean, i.e. anomalies.

Figures 10 and 11 show the two most important related patterns linking MSLP and cyclone frequency anomalies in the Pacific. The coefficient time series of the first (second) CCA pattern have a correlation of about 0.6 (0.4) and the pattern describes 48 % (35 %) of the variance of winter cyclone counts in the Pacific.

The first Pacific pattern (Fig. 10) is a unipolar pressure pattern with a center around the Aleutian Islands with minimum values below over −4.5 hPa. When the CCA coefficient is 1, then the maximum yearly mean Aleutian pressure anomaly is more than −4.5 hPa, the number of cyclones in cluster 4 is decreased by −0.6, in cluster 5 decreased by −2.2 and increased in cluster 6 by 4.6, on average. Thus, when the CCA pattern has a positive coefficient, the Aleutian Low tends to be stronger (lower pressure) and cyclone numbers of the eastern cluster 6 increase whereas cyclone counts in the western (cluster 4) and central (cluster 5) Pacific tend to be lower.

The second Pacific pattern (Fig. 11) describes a bipolar pressure pattern between the Aleutian Islands and North America with a pressure contrast of more than 3 hPa. This relates to a decrease/increase of cyclone counts in the western Pacific (cluster 4) but increase/decrease in the central (cluster 5) and eastern Pacific (cluster 6). This pattern seems to be related to the Pacific North American Oscillation (PNA) pattern, albeit with a shift, which is associated with the East Asian jet stream and influences cyclone genesis in the eastern Pacific (Sickmöller et al. 2000; Gulev et al. 2001) and cyclone activity in the western Atlantic (Christoph and Ulbrich 2000).

Figures 12 and 13 are the first and second CCA patterns for clusters 8, 9 and 10 over the Atlantic. The first pattern has a correlation of 0.5 for the coefficient time series and the second pattern shares a correlation of 0.3. They present about 39 and 31 %, respectively, of the variance for the year-to-year winter cyclone counts.

The first Atlantic pattern (Fig. 12) is a dipole located over the Iceland Low areas and the Atlantic subtropics with a pressure contrast of more than 4 hPa obviously related to the North Atlantic Oscillation (NAO) pattern with deeper/higher Iceland low and higher/shallower subtropical high. In the positive phase (deeper Icelandic Low) there are more cyclones for cluster 9 and cluster 10 over the southeast of Greenland and northeastern Atlantic, which agree with the study of Sickmöller et al. (2000). The NAO is known to be associated with variations of storm activity over the North Atlantic (Ulbrich and Chirstoph 1999; Sickmöller et al. 2000; Gulev et al. 2001; Pinto et al. 2007; Raible et al. 2007). When the NAO is in its positive phase, cold air from Arctic areas is encountering the warm North Atlantic current, and baroclinicity increases over the north Atlantic. This leads to more cyclone activity over the northeastern Atlantic. When the NAO is in its negative phase with a shallower Icelandic Low, cyclones shift southward and more intense cyclones happen in the Mediterranean area (Raible et al. 2007).

The second Atlantic pattern (Fig. 13) shows a unipolar pattern located over the Atlantic with values of more than −2.5 hPa. It relates that more cyclones show up along the eastern North Atlantic (cluster 10). And there are fewer cyclones over the coast of America (cluster 8) and over southern Greenland (cluster 9).

4 Conclusions

A coupled global atmosphere–ocean model (ECHO-G) simulation for the last about one thousand years was analyzed for changes in winter storm activity. The ECHO-G model was exposed to realistic variations of shortwave solar input, time-dependent presence of volcanic material in the upper atmosphere, and slowly changing greenhouse gas concentrations during the last millennium 1000–1990. An automatic tracking algorithm (Hodges 1994, 1995, 1999) was used to locate extratropical cyclones within the simulated MSLP fields. For validation reasons, the tracks were also compared with coarsened NCEP/NCAR reanalysis data. The main result of the study is that the time series of cyclone counts for years 1001 to 1990 show strong year to year variations, but an obvious trend was not found. The centennial variability of storm tracks is very small, whereas the centennial variation of hemispheric mean temperature is large.

Tracks were clustered into ten groups by applying the K-means method. The cluster results mainly correspond to the cyclone genesis areas. Frequency and distributions of lifetime as well as deepening rates were studied for the ten clusters. The oceanic cyclones show rapid deepening rates and a relatively long lifetime. Storm tracks in the Pacific are clustered into three groups: tracks over the western Pacific, in the central Pacific and in the eastern Pacific. In the Atlantic, tracks are also grouped into three clusters: tracks are located over the eastern North American coast, southern Greenland, and southeastern Iceland and the Norwegian Sea. The frequencies of cyclones in these two oceans are connected to large-scale pressure patterns. The main results for the Pacific and the Atlantic are concluded as follows:

The Pacific: Most cyclones are in the eastern Pacific, but fewest are in the central Pacific. Cyclones in the western Pacific survive longest (average lifetime of 6 days) and also show the highest percentage of cyclones lasting more than 10 days. Cyclones of the central Pacific have the highest proportions to deepen rapidly (>10 hPa per 12 h). In the 20th century those cyclones that deepen rapidly (>10 hPa per 12 h) become slightly more frequent over the western and central Pacific. Frequencies of cyclones over the western, central and eastern Pacific are correlated with each other and are also related to the Aleutian Low. When the Aleutian Low is stronger, cyclones in the eastern Pacific increase. Cyclones in the eastern Pacific show weak teleconnections across the American continent with cyclones in the Atlantic.

The Atlantic: Cyclones located over the eastern North American coast show the highest total numbers, the longest lifetimes with an average lifespan of 6 days, and also most cyclones which deepen rapidly (>10 hPa per 12 h) occur in this region. In the 20th century those rapidly deepening cyclones become less frequent over the eastern North American coast, but more frequent over southeastern Iceland and the Norwegian Sea. Cyclone counts over the Atlantic are correlated to the NAO pattern. During the positive NAO phase, there are more cyclones over the southeast of Greenland, the northeastern Atlantic and northwest Europe. Cyclone numbers over the Atlantic are smaller than for the Pacific. And more cyclones over the Pacific than over the Atlantic show a strong deepening rate of at least 10 hPa/12 h.

We conclude that this simulation of the last millennium shows only smaller variations on decadal to centennial time scales and no long-term trends for the whole period. This is valid for the location and numbers of cyclone tracks which are changing only marginally.

There are a number of caveats: First, the data are generated by a model as a response to prescribed, estimated external forcing (solar, volcanic material, greenhouse gases). These estimated external forcing factors may deviate from reality–discussions so far point more to an overestimation of solar and volcanic factors. If that would be so, then the conclusions of "little centennial variations of storm track statistics" would not be affected. Also the model may show too small variations of storm activity, in particular related to the coarse spatial resolution of only T30. Comparison with other studies indicates that there may be an underestimate, but this would be stationary in time, so that our conclusion about temporal variability would not be affected. Finally, the relatively infrequent storing of MSLP fields, only once in every 12 h, may have lead to too few detectable storms. We consider this possibility also less relevant, first because of successful previous studies with this "coarse" gridding. And again such a bias would hardly affect the strength of variations. But all in all, these caveats must be acknowledged, and future studies of similar millennial simulations, with better horizontal and temporal gridding, will show their significance.

Acknowledgments We thank Eduardo Zorita for providing ECHO-G simulation data, his support with statistic routines, and helpful discussions. We appreciate Kevin I. Hodges help with his tracking algorithm which was used for our study. The NCEP/NCAR reanalysis data were provided by the National Centre for Atmospheric Research (NCAR). We thank Beate Geyer for providing the NCEP/NCAR reanalysis data and technical supports. We also thank Beate Gardeike

for her help to prepare the figures. This work was funded by the China Scholarship Council (CSC) and the Institute of Coastal Research Helmholtz-Zentrum Geesthacht within the framework of the Junior Scientist Exchange Program organised by the CSC and the Helmholtz Association of German research centres (HGF). This work is a contribution to the "Helmholtz Climate Initiative REKLIM" (Regional Climate Change), a joint research project of HGF. The authors thank two anonymous reviewers for constructive comments that helped to improve this article.

References

Adachi S, Kimura F (2007) A 36-year climatology of surface cyclogenesis in East Asia using high-resolution reanalysis data. Sola 3:113–116

Alexandersson H, Schmith T, Iden K, Tuomenvirta H (1998) Longterm variations of the storm climate over NW Europe. Global Atmos Ocean Syst 6:97–120

Bender FA-M, Ramanathan V, Tselioudis G (2012) Changes in extratropical storm track cloudiness 1983–2008: observation support for a poleward shift. Clim Dyn 38:2037–2053

Bengtsson L, Hodges KI (2006) Storm tracks and climate change. J Clim 19:3518–3543

Blender R, Schubert M (2000) Cyclone tracking in different spatial and temporal resolutions. Mon Weather Rev 128:377–384

Blender R, Fraedrich K, Lunkeit F (1997) Identification of cyclone-track regimes in the North Atlantic. Q J R Meteorol Soc 123:727–741

Brayshaw DJ, Hoskin B, Blackburn M (2008) The storm-track response to idealized SST perturbations in an aquaplanet GCM. J Atmos Sci 65:2842–2860

Christoph M, Ulbrich U (2000) Can NAO-PNA relationship be established via the North Atlantic storm track? Geophys Res Abstr 2:215

Chu P, Zhao X, Kim J (2010) Regional typhoon activity as revealed by track patterns and climate change. Hurric Clim Change 2:137–148

Dierckx P (1981) An algorithm for surface fitting with spline functions. SIAM J Num Anal 19:1286–1304

Dierckx P (1984) Algorithms for smoothing data on the sphere with tensor product splines. Computing 32:319–342

Elsner JB (2003) Tracking hurricanes. Bull Am Meteorol Soc 84:353–356

Elsner JB, Liu K-B, Kocher B (2000) Spatial variations in major U.S. hurricane activity: statistics and a physical mechanism. J Clim 13:2293–2305

Fischer-Bruns I, von Storch H, González-Rouco JF, Zorita E (2005) Modelling the variablility of midlatitude storm activity on decadal to century time scales. Clim Dyn 25(5):461–476

González-Rouco F, von Storch H, Zorita E (2003) Deep soil temperature as proxy for surface air-temperature in a coupled model simulation of the last thousand years. Geophys Res Lett 30(21):2116

Gouirand I, Moron V, Zorita E (2007) Teleconnections between ENSO and North Atlantic in an ECHO-G simulation of the 1000–1990 period. Geophys Res Lett 34:L06705

Gulev SK, Zolina O, Grigoriev S (2001) Extratropical cyclone varibility in the Northern Hemisphere winter from the NCEP/NCAR reanalysis data. Clim Dyn 17:795–809

Hodges KI (1994) A general method for tracking analysis and its application to meteorological data. Mon Weather Rev 122:2573–2586

Hodges KI (1995) Feature tracking on the unit sphere. Mon Weather Rev 123:3458–3465

Hodges KI (1999) Adaptive constraints for feature tracking. Mon Weather Rev 127:1362–1373

Hoskins BJ, Hodges KI (2002) New perspectives on the Northern Hemisphere winter storm tracks. J Atmos Sci 59:1041–1061

Hoskins BJ, Hodges KI (2005) A new perspective on Southern Hemisphere storm tracks. J Clim 18:4108–4129

Hurrell JW (1995) Decadal trends in the North Atlantic Oscillation: regional temperatures and precipitation. Science 269:676–679

Inatsu M (2009) The neighbor enclosed area tracking algorithm for extratropical wintertime cyclones. Atmos Sci Lett 10:267–272

International Detection and Attribution Group (IDAG) (2005) Detecting and attributing external influences on the climate system: a review of recent advances. J Clim 18:1291–1314

Jung T, Gulev SK, Rudeva I, Soloviov V (2006) Sensitivity of extratropical cyclone characteristic to horizontal resolution in ECMWF model. Q J R Meteorol Soc 132:1839–1857

Kalnay E, Kanamitsu M, Kistler R, Collins W, Deaven D et al (1996) The NCEP/NCAR 40-year reanalysis project. Bull Am Meteorol Soc 77:437–471

Keigwin LD (1996) The little ice age and medieval warm period in the Sargasso Sea. Science 274:1503–1508

KIHZ-Consortium: Zinke J, von Storch H, Müller B, Zorita E, Rein B, Mieding HB, Miller H, Lücke A, Schleser GH, Schwab MJ, Negendank JFW, Kienel U, González-Rouco JF, Dullo C, Eisenhauser A (2004) Evidence for the climate during the late maunder minimum from proxy data available within KIHZ. In: Fischer H, Kumke T, Lohmann G, Flöser G, Miller H, von Storch H, Negendank JFW (eds) The climate in historical times. Towards a synthesis of Holocene proxy data and climate models, Springer, Berlin, 487 pp, ISBN 3-540-20601-9, pp 397–414

Matulla C, Schöner W, Alexandersson H, von Storch H, Wang XL (2008) European storminess: late nineteenth century to present. Clim Dyn 31:125–130

May W, Bengtsson L (1998) The signature of ENSO in the Northern Hemisphere midlatitude season mean flow and high-frequency intraseasonal variability. Meteorol Atmos Phys 69:81–100

Min SK, Legutke S, Hense A, Kwon WT (2005a) Internal variability in a 1000-yr control simulation with the coupled climate model ECHO-G. I: near-surface temperature, precipitation and mean sea level pressure. Tellus A 57:605–621

Min SK, Legutke S, Hense A, Kwon WT (2005b) Internal variability in a 1000-yr control simulation with the coupled climate model ECHO-G. II: El Niño Southern Oscillation and North Atlantic Oscillation. Tellus A 57:622–640

Moberg A, Sonechkin DM, Holmgren K, Datsenko NM, Karlén W (2005) Highly variable Northern Hemisphere temperatures reconstructed from low- and high-resolution proxy data. Nature 433:613–617

Murray RJ, Simmonds I (1991) A numerical scheme for tracking cyclone centres from digital data Part I: development and operation of the scheme. Aust Meteorol Mag 39:155–166

Muskulus M, Jacob D (2005) Tracking cyclones in regional model data: the future of Mediterranean storms. Adv Geosci 2:13–19

Nakamura J, Lall U, Kushnir Y, Camargo SJ (2009) Classifying North Atlantic tropical cyclone tracks by mass moments. J Clim 15:5481–5494

Pinto JG, Ulbrich U, Leckebusch GC, Spangehl T, Reyers M, Zacharias S (2007) Changes in storm track and cyclone activity in three SRES ensemble experiments with the ECHAM5/MPI-OM1 GCM. Clim Dyn 29:195–210

Raible CC, Blender R (2004) Northern Hemisphere Mid-latitude cyclone variability in different ocean representations. Clim Dyn 22:239–248

Raible CC, Yoshimori M, Stocker TF, Casty C (2007) Extreme midlatitude cyclones and their implications for precipitation and

wind speed extremes in simulations of the Maunder Minimum versus present day conditions. Clim Dyn 28:409–423

Roeckner E, Arpe K, Bengtsson L, Christoph M, Claussen M, Dümenil L, Esch M, Giorgetta M, Schlese U, Schulzweida U (1996) The atmopheric general circulation model ECHAM4: model description and simulation of present-day climate. Report No. 218, 90 pp, Max-Planck-Institut für Meteorologie, Bundesstr 55, Hamburg

Rudeva I, Gulev SK (2007) Climatology of cyclone size characteristic and their changes during the cyclone life cycle. Mon Weather Rev 135:2568–2587

Schubert M, Perlwitz J, Blender R, Fraedrich K, Lunkeit F (1998) North Atlantic cyclones in CO_2-induced warm climate simulations: frequency, intensity and tracks. Clim Dyn 14:827–837

Serreze MC (1995) Climatological aspects of cyclone development and decay in the arctic. Atmos-Ocean 33(1):1–23

Sickmöller M, Blender R, Fraedrich K (2000) Observed winter cyclone tracks in the northern hemisphere in re-analysed ECMWF data. Q J R Meteorol Soc 126:591–620

Stendel M, Roeckner E (1998) Impacts of horizontal resolution on simulated climate statistics in ECHAM4. Report No. 253, Max-Planck-Institut für Meteorologie, Bundesstr 55, Hamburg

Tan M, Shao X, Liu J, Cai B (2009) Comparative analysis between a proxy-based climate reconstruction and GCM-based simulation of temperature over the last millennium in China. J Quat Sci 24(5):547–551

Uccellini LW (1990) Process contributing to the rapid development of extratropical cyclones. In: Holopainen EO, Newton CW (eds) Extratropical cyclones. The Eric Palmen memorial volume. AMS, Boston, pp 81–106

Ulbrich U, Christoph M (1999) A shift of the NAO and increasing storm track activity over Europe due to anthropogenic greenhouse gas forcing. Clim Dyn 15:551–559

Ulbrich U, Leckebusch GC, Pinto JG (2009) Extra-tropical cyclones in the present and future climate: a review. Theor Appl Climatol 96:117–131

von Storch H, Zwiers FW (1999) Statistical analysis in climate research. Cambridge University Press, Cambridge

von Storch J-S, Kharin V, Cubasch U, Hegerl G, Schriever D, von Storch H, Zorita E (1997) A description of a 1260-year control integration with the coupled ECHAM1/LSG general circulation model. J Clim 10:1525–1543

von Storch H, Zorita E, Dimitriev Y, González-Rouco F, Tett S (2004) Reconstructing past climate from noisy data. Science 306:679–682

Weisse R, von Storch H, Feser F (2005) Northeast Atlantic and North Sea storminess as simulated by a regional climate model during 1958–2001 and comparison with observations. J Clim 18(3):465–479

Wernli H, Schwierz C (2006) Surface cyclones in the ERA-40 dataset (1958–2001). Part I: novel identification method and global climatology. J Atmos Sci 63:2486–2507

Wolff JO, Maier-Reimer E, Legutke S (1997) The Hamburg Ocean primitive equation model. Technical Report, No. 13, 98 pp, German Climate Computer Center (DKRZ), Hamburg

Xia L, Zahn M, Hodges KI, Feser F, von Storch H (2012) A comparison of two identification and tracking methods for polar lows. Tellus A 64:17196

Zahn M, von Storch H (2008a) Tracking polar lows in CLM. Meteorol Z 17(4):445–453

Zahn M, von Storch H (2008b) A long-term climatology of North Atlantic polar lows. Geophys Res Lett 35:L22702

Zolina O, Gulev SK (2002) Improving the accuracy of mapping cyclone numbers and frequencies. Mon Weather Rev 130:748–759

Zorita E, González-Rouco JF, von Storch H, Montávez JP, Valero F (2005) Natural and anthoropogenic model of surface temperature variations in the last thousand years. Geophys Res Lett 32:L08707